

GEOPHYSICS

Climbing the crustal ladder: Magma storage-depth evolution during a volcanic flare-up

Guilherme A. R. Gualda^{1*}, Darren M. Gravley², Michelle Connor¹, Brooke Hollmann¹, Ayla S. Pamukcu^{3,4†}, Florence Bégué⁵, Mark S. Ghiorso⁶, Chad D. Deering⁷

Very large eruptions (>50 km³) and supereruptions (>450 km³) reveal Earth's capacity to produce and store enormous quantities (>1000 km³) of crystal-poor, eruptible magma in the shallow crust. We explore the interplay between crustal evolution and volcanism during a volcanic flare-up in the Taupo Volcanic Zone (TVZ, New Zealand) using a combination of quartz-feldspar-melt equilibration pressures and time scales of quartz crystallization. Over the course of the flare-up, crystallization depths became progressively shallower, showing the gradual conditioning of the crust. Yet, quartz crystallization times were invariably very short (<100 years), demonstrating that very large reservoirs of eruptible magma were transient crustal features. We conclude that the dynamic nature of the TVZ crust favored magma eruption over storage. Episodic tapping of eruptible magmas likely prevented a supereruption. Instead, multiple very large bodies of eruptible magma were assembled and erupted in decadal time scales.

INTRODUCTION

Very large eruptions (>50 km³) and supereruptions (>450 km³) expel tens to thousands of cubic kilometers of magma onto Earth's surface in a matter of days to months (1), unambiguously revealing the capacity of Earth's shallow crust to store large quantities of eruptible magma (2). These magma bodies are predominantly—although not exclusively—crystal poor, as revealed by the generally low crystal contents [<25 weight % (wt %)] of the rocks formed from their eruptions. Eruptions of this magnitude—volcanic explosivity index ≥ 7 (3)—can be catastrophic to humankind at the local scale, with substantial global impact (1, 4). Yet, our understanding of the architecture of these systems and the processes associated with them is still limited. What are the mechanisms whereby Earth produces and collects such giant bodies of magma in relatively small areas that feed these eruptions? What are the time scales over which these bodies of magma evolve before eruption?

The current paradigm for the origin of rhyolites rests on the idea of segregation of crystal-poor magma from a crystal-rich reservoir, the so-called Mush model (5–7). Yet, the details of the depths at which extraction of the crystal-poor magma takes place, the geometry of the magma bodies that are thus established, and the connections between extracted and cumulate materials are still poorly understood. Recent work suggests that discrete bodies of crystal-poor, eruptible magma feed very large and supereruptions (8–11). Further, recent work reveals that the evolution of these magma bodies spans different time scales [see (12)]. The crystal-rich reservoir has a relatively extended life span, from tens to hundreds of thousands of years (13–16), possibly in excess of 1 million years (17)—as revealed, for instance, by time scales of zircon crystallization. However, the eruptible magma bodies—formed by extracted magma—that immediately

feed eruptions are much shorter lived, recording quartz crystallization over centuries to millennia (18–20). This short time scale suggests that once very large magma bodies are established, they are unstable features in the shallow crust (21) that are prone to erupting. To date, most studies of very large crystal-poor silicic deposits have focused on individual eruptions. Here, we explore the evolution of eruptible magma bodies and associated crustal maturation in a system where repeated very large eruptions took place in quick succession.

The Taupo Volcanic Zone (TVZ, New Zealand) is the volcanic region on Earth with the largest number of recent very large silicic caldera-forming eruptions (22). Over the last 350 thousand years (ka), more than 4000 km³ of magma have erupted in the TVZ, predominantly during eight very large eruptions (>50 km³ of ejected material in each) concentrated over only ~70 ka—a remarkable “ignimbrite flare-up” (23). This high productivity of silicic volcanism is linked to an intimate interplay between magmatic, tectonic, and volcanic processes (24); yet, evidence for these interacting processes has thus far been elusive. In this work, we explore the spatial and temporal variables that led to the accumulation and eruption of these very large bodies of eruptible magma in rapid succession. In the process, we gather critical information on the processes that lead to the formation of very large magma bodies during this flare-up, on the time scales of magma crystallization, and on the evolution of the shallow crust as heat and magma are transferred relatively rapidly into it. Our data reveal the interplay between crustal evolution and volcanism and also explain how magma distribution varied over this short (~70 ka) period within the central TVZ crust.

Over the span of ~10 ka (350–340 ka ago), during the first pulse of the TVZ flare-up (23), a series of very large to supersized eruptions led to the formation of the Whakamaru and Paeroa pyroclastic deposits (25)—more than 2000 km³ of material deposited through much of the central North Island (Fig. 1). With the end of the Whakamaru and Paeroa eruptions, major changes to the TVZ crust took place (23, 26). The second pulse of the flare-up was marked by a change in the character of the erupted magmas (23): Whakamaru and Paeroa (23) magmas were characteristically cooler, more hydrous (as revealed by the abundance of hornblende), and commonly saturated in both

Copyright © 2018
The Authors, some
rights reserved;
exclusive licensee
American Association
for the Advancement
of Science. No claim to
original U.S. Government
Works. Distributed
under a Creative
Commons Attribution
NonCommercial
License 4.0 (CC BY-NC).

¹Vanderbilt University, Earth and Environmental Sciences, PMB 351805, Nashville, TN, USA. ²University of Canterbury, Geological Sciences, Christchurch, New Zealand. ³Brown University, Providence, RI, USA. ⁴Princeton University, Princeton, NJ, USA. ⁵University of Lausanne, Institute of Earth Sciences, Lausanne, Switzerland. ⁶OFM Research-West, Seattle, WA, USA. ⁷Michigan Technological University, Houghton, MI, USA.

*Corresponding author. Email: g.gualda@vanderbilt.edu

†Present address: Woods Hole Oceanographic Institution, Geology & Geophysics, 266 Woods Hole Road, MS#08, Woods Hole, MA, USA.

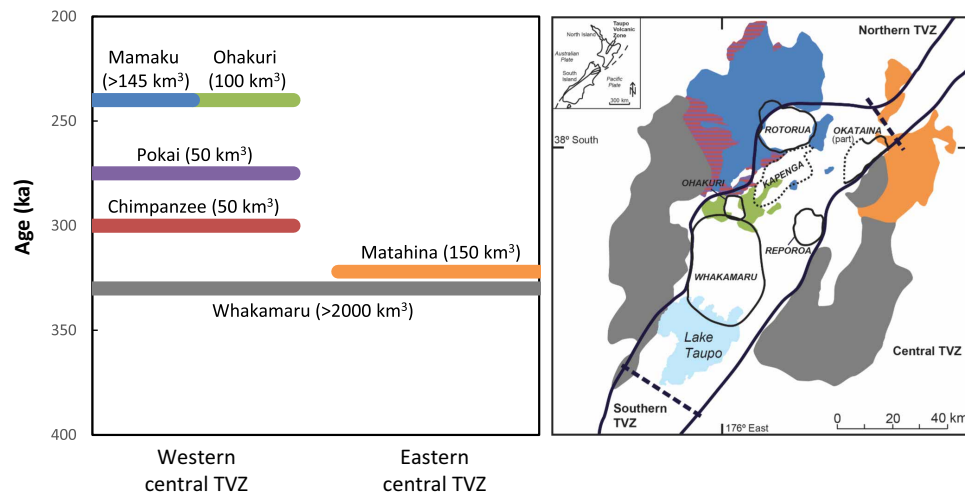


Fig. 1. Schematic showing the temporal evolution and map of the central TVZ highlighting the units of interest in this study. Key deposits are shown on both panels, with eruptive volumes indicated in parentheses on the left (see also table S1). In the left panel, the vertical position of each bar represents the best estimate for deposit age, while the horizontal position of bars depicts whether deposits are part of the western or eastern central TVZ, or both. Color of units in the map matches the colors on the diagram on the left.

sanidine and plagioclase; in contrast, magmas from the post-Whakamaru pulses 2 and 3 of the flare-up (23) were hotter and dryer, with plagioclase as the sole feldspar present (see table S1) (26). In pulse 2 (Matahina, Chimpanzee, and Pokai eruptions), rocks include rare hornblende and show transitional character (particularly Matahina), while in pulse 3 (Mamaku, Ohakuri, and Kaingaroa eruptions), the hot-dry assemblage with orthopyroxene as the dominant mafic mineral is characteristic (23).

Here, we use a multifaceted approach that capitalizes on matrix glass and mineral compositions to probe the depths and time scales of magma storage within the TVZ crust during flare-up volcanism. We focus on six eruptions (Whakamaru, Matahina, Chimpanzee, Pokai, Mamaku, and Ohakuri) that span the age and compositional spectrum of the TVZ flare-up. Our approach includes (i) rhyolite-MELTS geobarometry (27) to calculate the pressures at which crystallization took place in these eruptible magma bodies and reveal the vertical organization of magmas over time in the flare-up; (ii) determination of trace-element compositions of matrix glass to assess the compositional affinity of the various magmas that erupted during the flare-up; (iii) cathodoluminescence (CL) zoning and modeling of Ti diffusion in quartz to infer the time scales over which these segregated, crystal-poor bodies of eruptible magma resided in the shallow crust before eruption (18, 19); and (iv) phase-equilibria modeling with rhyolite-MELTS (28) to investigate crystallization histories and constrain the proportion of the total crystallization history recorded by quartz crystallization (19). In combination, these data lead to a comprehensive characterization of magma distribution in the shallow crust and of the rates of crystallization during the TVZ flare-up, with implications for understanding the evolving architecture of magmatic systems.

RESULTS

Magma crystallization depths can be calculated using the rhyolite-MELTS (28) geobarometer (27, 29, 30), by calculating the pressure at which an assemblage of quartz and feldspars last equilibrated with melt of composition equal to that of observed glass. We interpret these pressures as those at which crystal-poor, eruptible magma was

stored and crystallized before eruption. Our results using the rhyolite-MELTS geobarometer reveal a systematic spatial progression over the course of the flare-up (see Fig. 2). Our data suggest that Whakamaru magmas were stored and crystallized at pressures of <125 MPa. These relatively low pressures (~5 km depth assuming a shallow crust of 2700 kg/km³) are consistent with previous estimates (31) for Whakamaru (29), and they are typical of magma storage pressures in the central TVZ (29). Following a period of ~20 ka of relative quiescence, caldera-forming eruptions were fed from magma bodies stored at progressively lower pressures, particularly on the western side of the central TVZ. On the eastern side of the central TVZ, Matahina magmas were stored at pressures of 100 to 170 MPa; on the western side, Chimpanzee magmas were stored at higher pressures, primarily 180 to 270 MPa (one data point at 140 MPa). The western side of the central TVZ was the locus of renewed volcanism: The Chimpanzee eruption was followed by the Pokai eruption and then by the almost simultaneous Mamaku and Ohakuri eruptions (32). Storage depths decreased over time: Pokai records pressures between 150 and 190 MPa (and a second population of four data points with pressures of ~50 MPa); Mamaku records pressures of 50 to 160 MPa (one data point yielding 225 MPa); and pressures for Ohakuri are in the 50- to 100-MPa range. The lower pressures for Ohakuri and Mamaku are similar to those observed for Whakamaru and also typical of TVZ magmas (29).

Glass trace-element compositions reveal trends that are consistent with the patterns observed in crystallization pressures (Fig. 3). Matahina and Chimpanzee glass is the least evolved (e.g., higher Sr, lower LREE), while Mamaku and Ohakuri are the most evolved; Pokai glass compositions are generally intermediate between these two groups. Whakamaru glass shows compositions that do not align along the same trends (Fig. 3); this is likely due to the presence of sanidine, and it is consistent with the different nature of Whakamaru magmas (23, 26). Regardless of the mechanism that leads to such differences, we see an array of compositions that parallels the change in storage pressures over time.

We use quartz diffusion geochronometry using Ti concentration gradients (as revealed by CL zoning) in quartz crystals to probe crystallization times and growth rates during storage of crystal-poor,

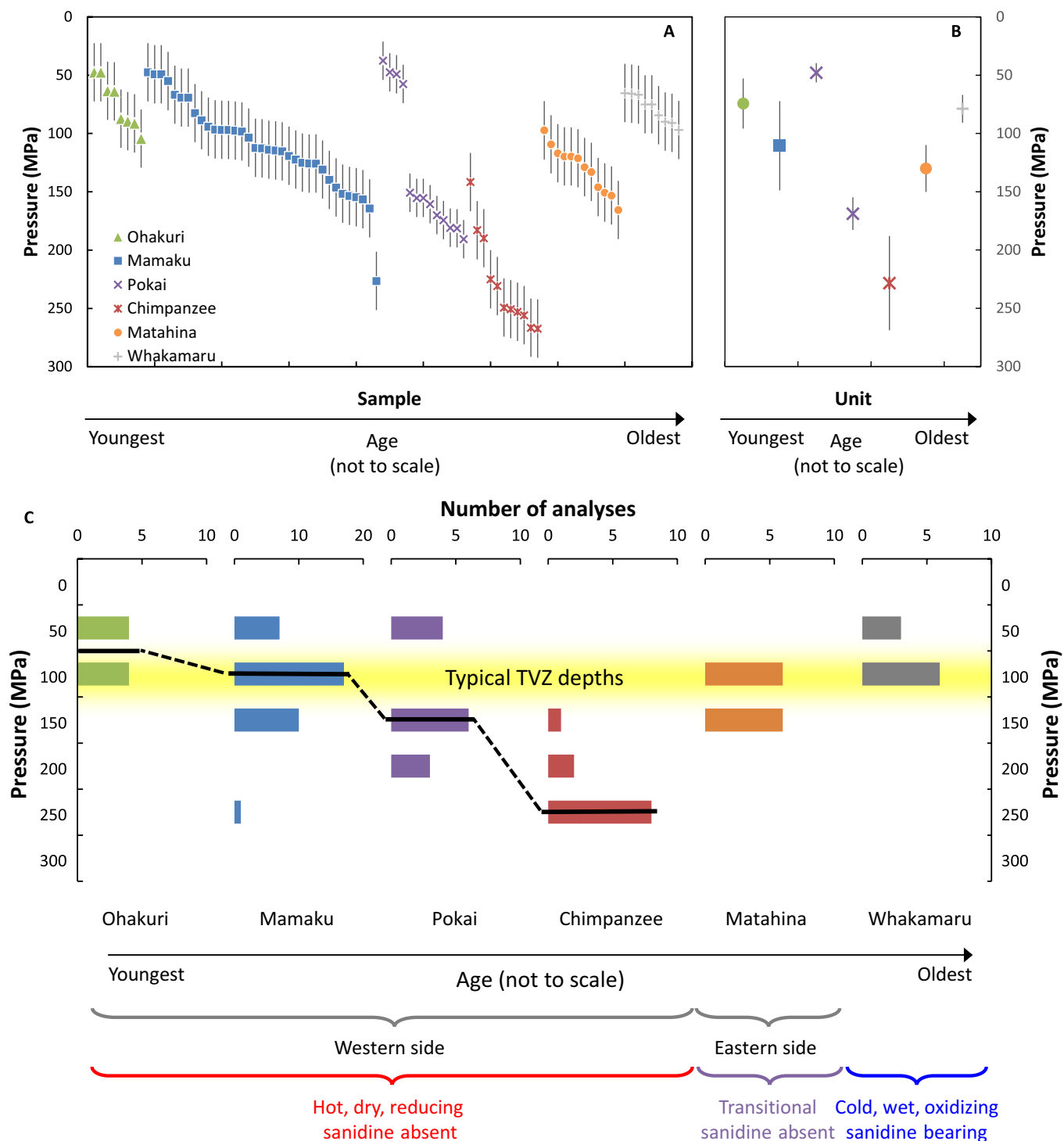


Fig. 2. Crystallization pressures for magmas of the TVZ volcanic flare-up and the late-Whakamaru group. (A) Each data point represents a single pressure determination based on rhyolite-MELTS calculations for a given matrix glass composition. Error bars are 25 MPa and represent our best estimate of the uncertainty associated with each determination (27). Different colors correspond to different eruptive units. Eruptive units are organized according to age (increasing to the right), but individual samples are ordered according to crystallization pressure to facilitate visualization. (B) Each data point represents the average of all determinations for the corresponding unit (or subunit, in the case of Pokai); error bars are the SD associated with that average. Units are organized according to age, like in (A); the ordering of Pokai subunits is arbitrary, with shallower subunits shown to the left for ease of visualization. (C) Bar diagrams of crystallization pressure for each unit. Diagrams are organized in order of increasing age, but age is not to scale. The vertical (pressure) axis is the same for all diagrams. The horizontal (number of analyses) scale is the same for all diagrams, except for Mamaku rocks, as indicated. The vertical (pressure) axis is the same for all diagrams. The horizontal (number of analyses) scale is the same for all diagrams. The data reveal a time progression for the storage depths of magmas feeding flare-up eruptions, particularly for the hot-dry-reducing magmas in the western portion of the central TVZ: Storage starts at relatively deep levels for Chimpanzee magmas and gradually becomes shallower until the co-eruption of Mamaku and Ohakuri magmas.

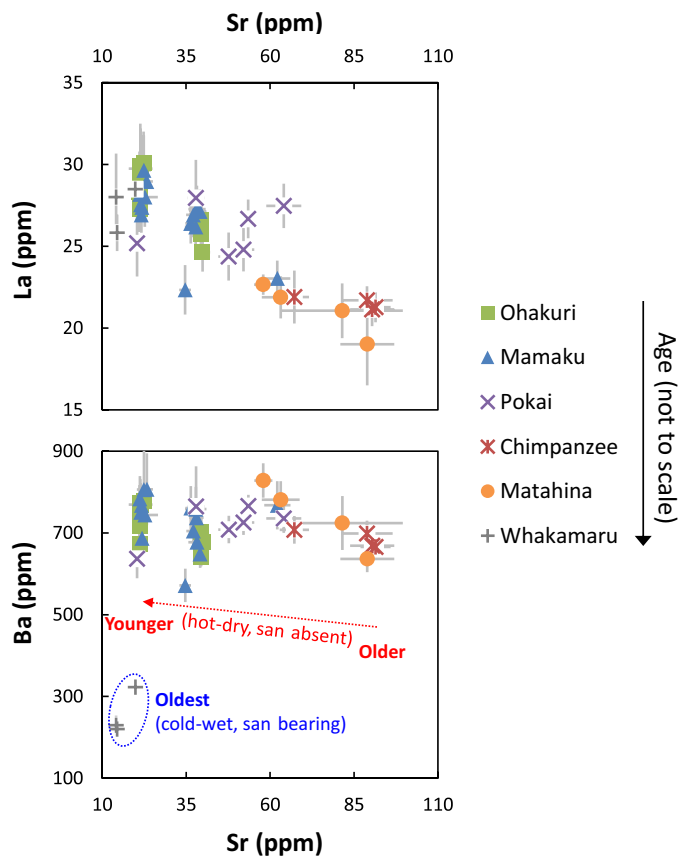


Fig. 3. Trace-element plots showing the compositional evolution of flare-up magmas in comparison with late-Whakamaru magmas. Whakamaru glass has very distinct Ba contents, probably a consequence of equilibration with sanidine. Flare-up magmas form a distinct array, with glass from older units (e.g., Chimpanzee) being less evolved [i.e., lower light rare earth element (LREE) and higher Sr] than glass from younger units (e.g., Ohakuri), paralleling the time progression observed in crystallization pressures. ppm, parts per million.

eruptible magmas that fed these eruptions (Fig. 4) (12, 18, 19). The origin of CL zoning in quartz is contentious [see (12)]—while a common interpretation is that Ti correlates with temperature variations (33, 34), it is now clear that Ti zonation can also result from variations in pressure (35, 36) and growth rate (37, 38). Nonetheless, regardless of the specific origin, the existence of different zones in quartz allows determination of crystallization times [see (18)]. In high-silica rhyolite magmas like the ones studied here, the quartz stability field is only reached after crystallization of a feldspar (39), such that quartz is likely to be consumed during waxing stages of a longer-lived magmatic system. In this sense, quartz differs substantially from zircon and feldspars, which show substantial inheritance (14, 40–42) and record the more extended history of waxing and waning of the magmatic systems in which they crystallize (12, 18). As a result, quartz records crystallization only after establishment of very large crystal-poor, eruptible magma bodies (12, 18, 19)—the magmas that ultimately feed eruptions. Even if quartz were to be partly inherited, the crystallization times we determine are overestimates of the time scales of the magma bodies that feed eruptions (18, 19).

In contrast to crystallization pressures and glass trace-element compositions, which vary substantially and systematically over time,

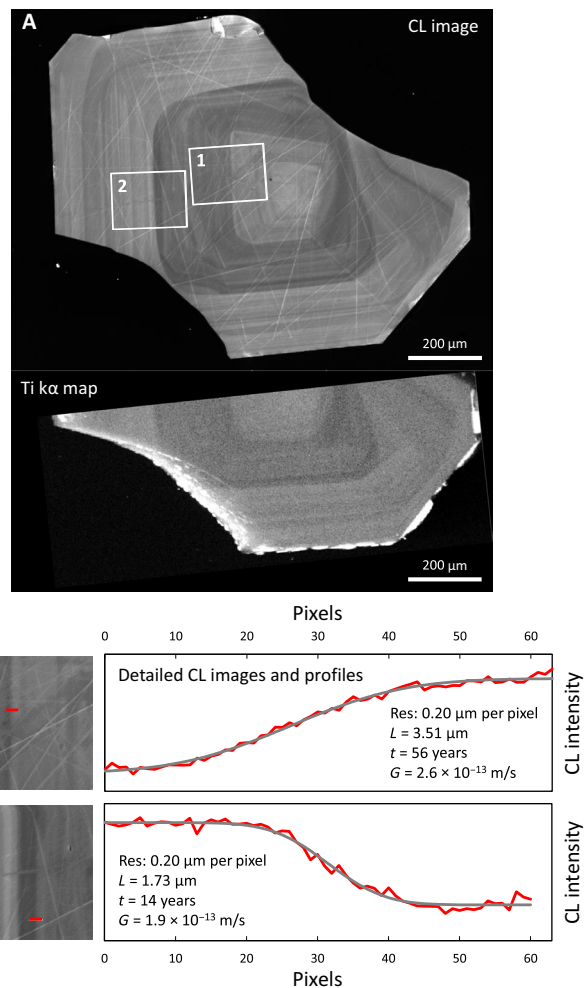


Fig. 4. Example of CL and Ti zoning in quartz, including calculation of growth time and rate from detailed CL images. CL image and Ti map shown in (A) demonstrate the correlation between CL intensity and Ti contents in quartz when there are large changes in CL; it can be seen that CL images capture the zoning in more detail, justifying the use of CL images for crystallization time and growth rate determination. Two areas were selected for detailed CL imaging, as indicated. (B) Detailed CL images with corresponding profiles used for calculations of crystallization time and growth rate. Each observed profile (red curve) is the average of 11 parallel profiles obtained from the image (shown in red in the corresponding image). The best-fit error function is shown in gray, from which the characteristic diffusion length (L) is extracted, which allows calculation of crystallization times (t). Calculation of growth rate (G) requires obtaining the distance between the boundary and the edge of the crystal from the larger CL image. See text for more details.

particularly on the western central TVZ, crystallization times and average quartz growth rates are similar for all units studied (Fig. 5). For all units, calculated maximum crystallization times have modes between 10 and 100 years. The longest calculated time is 273 years, but 84% of all the calculated times are within 100 years before eruption. These results are consistent with existing results for Whakamaru magmas (20, 43). Resulting growth rates are also all very similar, with 74% of the calculated growth rates between 10^{-12} and 10^{-13} m/s (~ 100 to 10 nm/day), similar to existing estimates for other systems (19). At these growth rates, a 1-mm-diameter crystal (typical maximum size

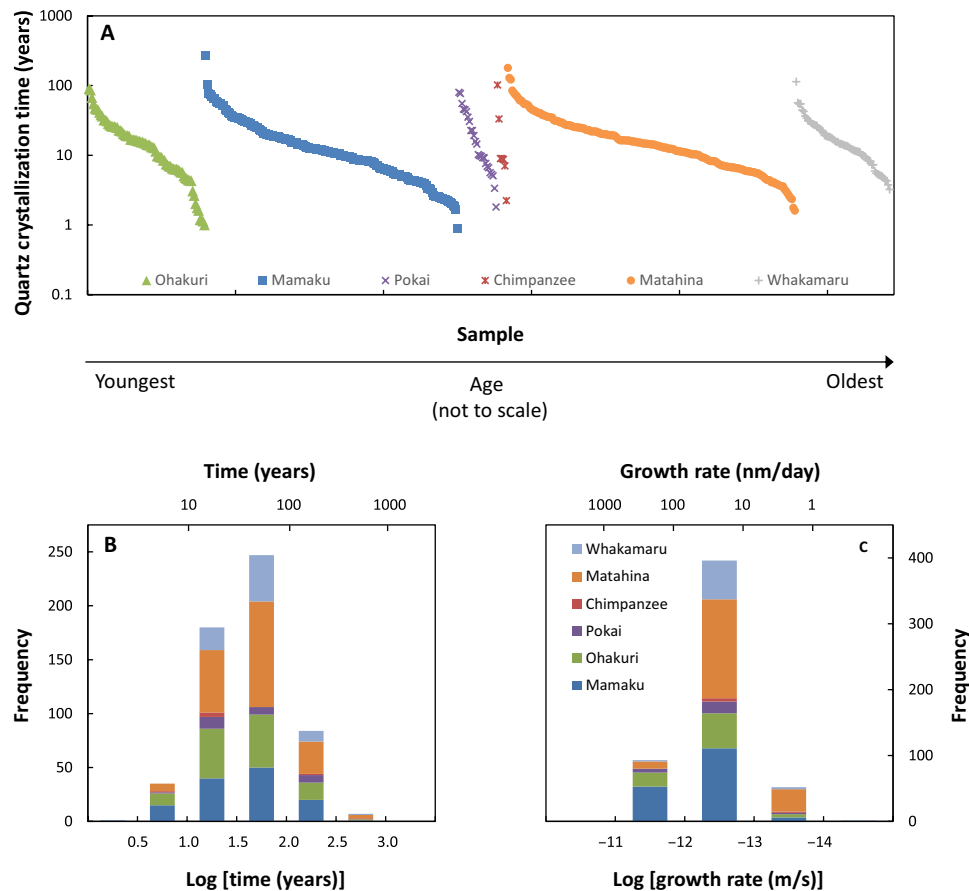


Fig. 5. Calculated crystallization times and growth rates for quartz from the TVZ volcanic flare-up and the late-Whakamaru group deposits. (A) Each data point represents an individual determination from a crystal from the corresponding unit. Units are organized according to age (increasing to the right), but individual data points for each unit are placed in order of increasing time to facilitate visualization. (B) Histogram showing distribution of crystallization times for each unit. (C) Histogram showing distribution of growth rates for each unit. The range of times is almost invariably within 1 and 100 years for all units, and growth rates are the same for all units.

in the studied rocks) would grow in ~ 300 years, placing a maximum bound on the crystallization times for the units studied here.

Given that quartz is not the first phase to crystallize in rhyolitic magmas (39), we complement the quartz geochronometry data with rhyolite-MELTS simulations. Our goal is to assess the amount of crystallization—and the total time associated with it—that occurred before quartz saturation (18, 19). We assume that heat loss by a magma body is nearly constant over time, such that crystallization time is proportional to enthalpy change [see (18, 19)], which can be calculated using rhyolite-MELTS. The observed crystal contents in pumice can be used to constrain the total enthalpy loss, and the fraction of time before quartz saturation is given by the fraction of enthalpy lost in that crystallization span (18, 19). We assume that these magmas behaved as closed systems, which is consistent with the low crystal contents ($<10\%$ crystals) of the erupted pumice studied here [see (19)]. Our results demonstrate that in the studied high-silica rhyolites, quartz saturation takes place at low total crystal content values (Fig. 6). Comparison of results from rhyolite-MELTS with observed crystal contents in pumice suggests that quartz was present in the crystallizing assemblage from 100 to 10% of the total crystallization time. This suggests that, in the worst-case scenario, quartz crystallization times represent 10% of the total crystallization time, which leads to the conclusion that total crystallization time was no more than a millen-

nium for the systems studied here. For the most part, crystallization times are likely much shorter than a millennium, possibly as short as decades. Centennial to millennial time scales are typical of other systems (18–20), which makes the decadal time scales determined here particularly short.

DISCUSSION

In combination, these data suggest both a dramatic change in magma storage following the Whakamaru and Paeroa eruptions and a time progression in storage levels during pulses 2 and 3 of the TVZ flare-up. The changes in crystallization pressure and glass compositions from Whakamaru and Paeroa to pulse 2 magmas (i.e., Chimpanzee and Matahina rocks) are consistent with the idea that the Whakamaru magma system shut down at the end of the Whakamaru and Paeroa eruptions and was replaced by a new magmatic system (26). Our data reveal that subsequent to the shutdown of the Whakamaru and Paeroa magmatic system, new magmas were emplaced, crystallized, and fed eruptions from deeper regions in the crust, forming the units of pulse 2. With time, storage conditions became shallower, until pressures more typical of the central TVZ were established at the time of the Ohakuri and Mamaku eruptions (pulse 3). The shallower Pokai population may demonstrate early establishment of shallow magma bodies.

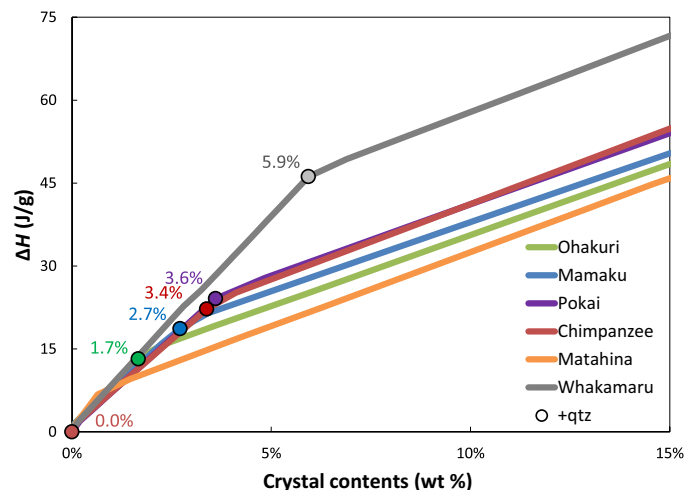


Fig. 6. Results of rhyolite-MELTS simulations showing the enthalpy lost over the course of crystallization for magmas from the TVZ volcanic flare-up and the late-Whakamaru group deposits. Each curve corresponds to the enthalpy loss from liquidus (crystal-free) conditions to 15 wt % crystals. Plagioclase is a liquidus phase in all cases. The data points in each curve represent the crystal content and enthalpy at which the system saturates in quartz (qtz) for that composition. Pressures used are the average for each unit (Fig. 2B). Water contents are set to yield fluid saturation at the liquidus, and f_{O_2} is set to the Ni-NiO buffer. Starting compositions and pressure used are given in table S2. Pumice from the TVZ flare-up typically contains <10 wt % crystals, suggesting that measured quartz growth times (Fig. 5) in general correspond to at least 25% of the total crystallization times (under the limiting assumption that magmas were initially crystal free). For Whakamaru, crystal contents can be as high as 25 wt % crystals. This suggests that crystallization times based on quartz crystallization times are typically within a factor of 4, and no more than within a factor of 10, of the total crystallization time.

This evolution in the storage depths of magmas (particularly on the western central TVZ, from Chimpanzee to Ohakuri) suggests eruptions emanating from new magma bodies that assembled quickly as heat transfer from the deep crust remained high following Whakamaru volcanism. The exact mechanisms that lead to this evolution in storage depths are not entirely understood. On the one hand, the shallowing progression may have resulted from external forcing, for instance, due to changes in the tectonic controls imposed by crustal extension (24, 44). However, they can also have been controlled internally, in response to the gradual conditioning of the crust due to the repeated intrusion of magma (45) and consequent heat transfer into it (44). Most likely, both factors have played their part, in which case what our data reveal is a ladder-like evolution of magma storage depths as a result of the interplay between tectonics and magmatism over time. This interplay between geologic processes has been hypothesized and modeled for the TVZ (24, 45), but we present tangible evidence for the first time.

The crystallization time scales we derive from quartz diffusion geochronometry reveal the time scales over which storage and crystallization of crystal-poor, eruptible magma take place—i.e., once established, coherent bodies of crystal-poor magma reside in the shallow crust until they ultimately feed eruptions, and we probe the time frame between establishment of these bodies of magma and eruption (12, 18, 19). Our results show extremely short storage times for these eruptible magmas in the TVZ crust, on predominantly decadal time scales. Even after correction for the crystallization interval in which quartz was absent, storage times are still at most within centuries. This shows

that these bodies of eruptible magma were somewhat transient features of the TVZ crust (18, 19). These time scales are much shorter than the intervals between successive eruptions, suggesting that the eruptible magma bodies that fed these eruptions never coexisted. The unimodal distribution of crystallization pressures for any given eruption suggests that these eruptions did not result from direct mobilization and eruption of magmas from a dispersed source region (11). Rather, crystal-poor magmas were collected and remained stored—albeit briefly—in coherent bodies from which eruptions were sourced. The evidence points to sill-like bodies that span a narrow depth range, but more work is needed to better constrain the geometry of these magma bodies. The collection and storage of magmas in relatively shallow, discrete bodies are consistent also with the subsidence invariably observed following eruption and caldera collapse in the central TVZ (46, 47). Yet, the depths and time scales over which the segregation, collection, and extraction (from a deeper crystal-rich reservoir) of magma responsible for the establishment of these eruptible magma bodies are poorly understood because of the lack of appropriate geobarometers and geochronometers that provide information on this stage of evolution.

The short lifetimes of the flare-up magma bodies following the Whakamaru event seem to indicate that conditions were ripe for eruption; whether—or, perhaps better stated, regardless of the extent to which—eruptions were internally triggered or externally assisted (21, 48–50), the conclusion is that the central TVZ crust was rather unstable during flare-up volcanism, favoring magma eruption over prolonged storage. We speculate that this dynamic tectono-magmatic environment prevented the buildup of a post-Whakamaru supereruption-size magma body (or set of magma bodies) in the central TVZ, and it favored eruption of smaller batches of magma. Had conditions been more stable, greater volumes of magma could have accumulated and been stored in the crust, potentially leading to the establishment of a supereruption-size body of eruptible magma. In this supereruptive scenario, the volume of magma would likely have waxed and waned over time (18, 40), leading to a more complex mosaic of multiple coexisting magma bodies, of variable dimensions, located over a wider range of depths (11). There is growing evidence that eventual destabilization and eruption of such mosaics of magma bodies are characteristic of supereruptions (8–10), even if the relatively organized sequential tapping of these magma bodies may appear to indicate the presence of a single, large, zoned magma body.

In combination, our data suggest establishment of discrete bodies of eruptible magma located at specific depths in the shallow crust. These bodies are rather unstable features of the shallow crust, and they are prone to eruption by their own evolution (21, 48). This is consistent with recent work (18, 19, 51, 52) that demonstrates that supereruption-forming magma bodies are ephemeral, being stored for no more than centuries to a few millennia before eruption. That is, magma storage and eruption can happen on historical time scales. What we argue here is that, under special circumstances, very large (>50 km³) bodies of eruptible magma can develop even faster, leading to storage and eruption over decadal—that is, human lifetime—time scales. What emerges is a scenario in which the central TVZ was a rapidly evolving system after the Whakamaru and Paeroa eruptions, with rapid magma generation, storage, and eruption, under varying conditions, as a response to the continuous transfer of heat and mass to the shallow crust.

Last, understanding the organization of magma bodies in the crust and the time scales over which they evolve can ultimately prove relevant

for hazard assessment and mitigation. Rapid magma evolution as seen in the case of the TVZ flare-up is seen in places where magmatic activity was persistent for much longer periods of time—as revealed, for instance, in the form of recurrent volcanism (e.g., TVZ) or a much longer record of crystallization preserved in zircon from the same system [e.g., Long Valley, California (13) and Whakamaru, TVZ (16)]. Given the magnitude of the potential impact of a supereruption on society, we suggest that monitoring of potentially restless calderas must include the specific search for clues that reveal mobilization and storage of large quantities of magma on time frames of multiple years to decades.

MATERIALS AND METHODS

We studied a total of 51 pumice clasts from six deposits (from older to younger; see Fig. 1): Whakamaru, Matahina, Chimpanzee, Pokai, Mamaku, and Ohakuri. Pumice clasts were lightly crushed using a baseball bat; after sieving, each size fraction was winnowed in water to separate crystal-rich from glass-rich fractions (53). Glass-coated, preferably whole, quartz crystals were handpicked from the crystal-rich fractions and mounted in epoxy; mounts were ground to expose crystal interiors and polished down to 1- μm grit for CL imaging (18). We also prepared epoxy mounts of pieces of vesiculated glass from the glass-rich fractions for matrix glass analysis.

We used a Tescan VEGA3 scanning electron microscope with an attached panchromatic Tescan CL detector for CL imaging and an Oxford X-max 50-mm² energy-dispersive spectrometry (EDS) system for major-element compositional analysis. We used a 15-kV beam with specimen currents on the order of 3 nA for both CL imaging and EDS analysis. For CL imaging, we used a dwell time of 1 ms per pixel. For EDS analysis, we used live acquisition times of 25 s, so as to minimize Na loss but yield measurable amounts (i.e., above quantification limit) of minor elements, particularly Ti and Mg, which appear in concentrations between 0.1 and 0.5 oxide wt %. The quality of the resulting analysis was checked by analyzing glass synthesized in the laboratory using the U.S. Geological Survey reference powder RGM-1 (54); results by Pamukcu *et al.* (30), using the same instrument and conditions, demonstrate that our EDS analyses compare very well with reference values for RGM-1.

We used x-ray microfluorescence (55) to obtain Ti maps on a subset of quartz crystals to investigate the correlation between CL intensity and Ti concentration. The x-ray microprobe at GeoSoilEnviroCARS uses the insertion device beamline 13IDC at the Advanced Photon Source (Argonne National Laboratory). We followed the procedures described in (12). The resolution of the obtained Ti maps is <5 μm per pixel.

We used a ThermoFisher iCAP Qc quadrupole inductively coupled plasma mass spectrometer (ICP-MS) coupled with a Photon Machines Excite 193-nm excimer laser ablation system (LA-ICPMS) for trace element analysis of matrix glass. The laser was set to a fluence of $\sim 6 \text{ J/cm}^2$, a repetition rate of 10 Hz, and a diameter of 50 μm , with He as carrier gas. Total analysis time was 90 s, including 20 s of pre-ablation, 60 s of ablation, and a 10-s interval before the next analysis. We used National Institute of Standards and Technology (NIST) 612 (56) as a primary standard and NIST 614 (57) and RGM-1 as secondary standards. We analyzed primary and secondary standards every 20 to 30 unknown measurements. Data processing was performed with the program Glitter (58), using Si as an internal standard. At least 20 analyses of glass in each sample were obtained, and results were averaged after excluding outliers (primarily due to mineral inclusions) (59).

Magma crystallization depths were calculated with the rhyolite-MELTS geobarometer (27, 28) using the measured major-element glass compositions, as the pressures at which quartz and plagioclase are in equilibrium with a melt of the analyzed composition (27). A total of 88 of 144 compositions yielded crystallization pressures, consistent with previous applications of the rhyolite-MELTS geobarometer (10, 27, 29, 30).

Crystallization time scales and average quartz growth rates were calculated using CL zoning as a proxy for Ti zoning (18, 19, 60). We assumed that profiles were initially step functions and calculated diffusion times using a one-dimensional diffusion model from best-fit curves to measured profiles (18, 19); the assumption of a step function assures that we calculate maximum times for a given temperature, given that initial profiles may have been smoother than assumed. We used a set of routines developed in-house to extract intensity profiles from CL images and fit the appropriate error function to the extracted profiles. In all cases, we assumed a temperature of 775°C, consistent with existing temperature estimates for Whakamaru magmas (31, 43) and appropriate for all flare-up magmas. We calculated diffusion coefficients for Ti in quartz following the experimental work of Cherniak *et al.* (61). Uncertainties in the diffusion coefficient derive from the uncertainty in the activation energy, which is <5% 1 σ (61) but appears in the exponential term of the diffusion equation, and uncertainties in temperature, which we assume to be 25°C 1 σ so as to encompass a wide range of possible temperatures (725° to 825°C at the 2- σ level). Following Gualda *et al.* (18), resulting errors in the calculated times are on the order of 150%; this level of uncertainty is small compared to other sources of error. Average growth rates (G) were calculated as the ratio between the growth distance (L) measured in the CL images (i.e., the distance between the zone boundary used for time estimates and the nearest crystal edge) and the growth time (t) calculated from the CL profiles (i.e., $G = L/t$; see Fig. 5) (12, 18, 19).

Rhyolite-MELTS (28) simulations were performed using MELTS_Excel (62). For each studied unit, we calculated an average of high-silica rhyolite compositions from data presented by Gravley *et al.* (23) (table S2). Isobaric crystallization simulations were performed from liquidus to near solidus (~ 10 wt % liquid left), at pressures calculated here for that unit, assuming water saturation and an f_{O_2} of NNO. The goal of the simulations was to determine the extent of crystallization of each magma before saturation in quartz. The choice of f_{O_2} is not particularly important for these SiO₂-rich, low-FeO, low-MgO magmas (28, 63).

SUPPLEMENTARY MATERIALS

Supplementary material for this article is available at <http://advances.sciencemag.org/cgi/content/full/4/10/eaap7567/DC1>

Table S1. Characteristics of eruptive deposits from the central TVZ analyzed in this study.

Table S2. Magma compositions used for rhyolite-MELTS modeling of energy change associated with crystallization.

Data file S1. Includes supplementary tables S3 to S5.

REFERENCES AND NOTES

1. J. B. Lowenstern, R. B. Smith, D. P. Hill, Monitoring super-volcanoes: Geophysical and geochemical signals at Yellowstone and other large caldera systems. *Philos. Trans. A Math. Phys. Eng. Sci.* **364**, 2055–2072 (2006).
2. C. F. Miller, D. A. Wark, Supervolcanoes and their explosive supereruptions. *Elements* **4**, 11–15 (2008).
3. C. G. Newhall, S. Self, The Volcanic Explosivity Index (VEI): An estimate of explosive magnitude for historical volcanism. *J. Geophys. Res. Oceans* **87**, 1231–1238 (1982).
4. S. Self, The effects and consequences of very large explosive volcanic eruptions. *Philos. Trans. A Math. Phys. Eng. Sci.* **364**, 2073–2097 (2006).

5. O. Bachmann, G. W. Bergantz, On the origin of crystal-poor rhyolites: Extracted from batholithic crystal mushes. *J. Petrol.* **45**, 1565–1582 (2004).
6. O. Bachmann, G. W. Bergantz, Rhyolites and their source mushes across tectonic settings. *J. Petrol.* **49**, 2277–2285 (2008).
7. O. Bachmann, G. W. Bergantz, The magma reservoirs that feed supereruptions. *Elements* **4**, 17–21 (2008).
8. G. F. Cooper, C. J. N. Wilson, M.-A. Millet, J. A. Baker, E. G. C. Smith, Systematic tapping of independent magma chambers during the 1 Ma Kidnappers supereruption. *Earth Planet. Sci. Lett.* **313–314**, 23–33 (2012).
9. F. Bégué, C. D. Deering, D. M. Gravelly, B. M. Kennedy, I. Chambeform, G. A. R. Gualda, O. Bachmann, Extraction, storage and eruption of multiple isolated magma batches in the paired mamaku and ohakuri eruption, Taupo Volcanic Zone, New Zealand. *J. Petrol.* **55**, 1653–1684 (2014).
10. G. A. R. Gualda, M. S. Ghiorso, The Bishop Tuff giant magma body: An alternative to the Standard Model. *Contrib. Mineral. Petrol.* **166**, 755–775 (2013).
11. K. V. Cashman, G. Giordano, Calderas and magma reservoirs. *J. Volcanol. Geotherm. Res.* **288**, 28–45 (2014).
12. G. A. R. Gualda, S. R. Sutton, The year leading to a supereruption. *PLOS ONE* **11**, e0159200 (2016).
13. J. I. Simon, M. R. Reid, The pace of rhyolite differentiation and storage in an ‘archetypical’ silicic magma system, Long Valley, California. *Earth Planet. Sci. Lett.* **235**, 123–140 (2005).
14. B. L. A. Charlier, C. J. N. Wilson, J. B. Lowenstern, S. Blake, P. W. V. A. N. Calsteren, J. P. Davidson, Magma generation at a large, hyperactive silicic volcano (Taupo, New Zealand) revealed by U-Th and U-Pb systematics in zircons. *J. Petrol.* **46**, 3–32 (2005).
15. C. J. N. Wilson, B. L. A. Charlier, Rapid rates of magma generation at contemporaneous magma systems, Taupo Volcano, New Zealand: Insights from U-Th model-age spectra in Zircons. *J. Petrol.* **50**, 875–907 (2009).
16. S. J. A. Brown, I. R. Fletcher, SHRIMP U-Pb dating of the preeruption growth history of zircons from the 340 ka Whakamaru Ignimbrite, New Zealand: Evidence for > 250 ky. magma residence times. *Geology* **27**, 1035–1038 (1999).
17. J. F. Kaiser, S. de Silva, A. K. Schmitt, R. E. Conomos, M. Sunagua, Million-year melt-presence in monotonous intermediate magma for volcanic-plutonic assemblage in the Central Andes: Contrasting histories of crystal-rich and crystal-poor super-sized silicic magmas. *Earth Planet. Sci. Lett.* **457**, 73–86 (2017).
18. G. A. R. Gualda, A. S. Pamukcu, M. S. Ghiorso, A. T. Anderson Jr., S. R. Sutton, M. L. Rivers, Timescales of quartz crystallization and the longevity of the Bishop giant magma body. *PLOS ONE* **7**, e37492 (2012).
19. A. S. Pamukcu, G. A. R. Gualda, F. Bégué, D. M. Gravelly, Melt inclusion shapes: Timekeepers of short-lived giant magma bodies. *Geology* **43**, 947–950 (2015).
20. N. E. Matthews, C. Huber, D. M. Pyle, V. C. Smith, Timescales of magma recharge and reactivation of large silicic systems from Ti diffusion in quartz. *J. Petrol.* **53**, 1385–1416 (2012).
21. L. Caricchi, C. Annen, J. Blundy, G. Simpson, V. Pintel, Frequency and magnitude of volcanic eruptions controlled by magma injection and buoyancy. *Nat. Geosci.* **7**, 126–130 (2014).
22. C. J. N. Wilson, B. F. Houghton, M. O. McWilliams, M. A. Lanphere, S. D. Weaver, R. M. Briggs, Volcanic and structural evolution of Taupo Volcanic Zone, New Zealand: A review. *J. Volcanol. Geotherm. Res.* **68**, 1–28 (1995).
23. D. M. Gravelly, C. D. Deering, G. S. Leonard, J. V. Rowland, Ignimbrite flare-ups and their drivers: A New Zealand perspective. *Earth Sci. Rev.* **162**, 65–82 (2016).
24. C. Wilson, D. M. Gravelly, G. S. Leonard, J. Rowland, Volcanism in the central Taupo Volcanic Zone, New Zealand: Tempo, styles, and controls. *Spec. Publ. IAVCEI* **2**, 225–247 (2009).
25. S. J. A. Brown, C. J. N. Wilson, J. W. Cole, J. Wooden, The Whakamaru group ignimbrites, Taupo Volcanic Zone, New Zealand: Evidence for reverse tapping of a zoned silicic magmatic system. *J. Volcanol. Geotherm. Res.* **84**, 1–37 (1998).
26. C. D. Deering, D. M. Gravelly, T. A. Vogel, J. W. Cole, G. S. Leonard, Origins of cold-wet-oxidizing to hot-dry-reducing rhyolite magma cycles and distribution in the Taupo Volcanic Zone, New Zealand. *Contrib. Mineral. Petrol.* **160**, 609–629 (2010).
27. G. A. R. Gualda, M. S. Ghiorso, Phase-equilibrium geobarometers for silicic rocks based on rhyolite-MELTS. Part 1: Principles, procedures, and evaluation of the method. *Contrib. Mineral. Petrol.* **168**, 1033 (2014).
28. G. A. R. Gualda, M. S. Ghiorso, R. V. Lemons, T. L. Carley, Rhyolite-MELTS: A modified calibration of MELTS optimized for silica-rich, fluid-bearing magmatic systems. *J. Petrol.* **53**, 875–890 (2012).
29. F. Bégué, G. A. R. Gualda, M. S. Ghiorso, A. S. Pamukcu, B. M. Kennedy, D. M. Gravelly, C. D. Deering, I. Chambeform, Phase-equilibrium geobarometers for silicic rocks based on rhyolite-MELTS. Part 2: Application to Taupo Volcanic Zone rhyolites. *Contrib. Mineral. Petrol.* **168**, 1082 (2014).
30. A. S. Pamukcu, G. A. R. Gualda, M. S. Ghiorso, C. F. Miller, R. G. McCracken, Phase-equilibrium geobarometers for silicic rocks based on rhyolite-MELTS-Part 3: Application to the Peach Spring Tuff (Arizona-California-Nevada, USA). *Contrib. Mineral. Petrol.* **169**, 33 (2015).
31. N. E. Matthews, D. M. Pyle, V. C. Smith, C. J. N. Wilson, C. Huber, V. van Hinsberg, Quartz zoning and the pre-eruptive evolution of the similar to 340-ka Whakamaru magma systems, New Zealand. *Contrib. Mineral. Petrol.* **163**, 87–107 (2012).
32. D. M. Gravelly, C. J. N. Wilson, G. S. Leonard, J. W. Cole, Double trouble: Paired ignimbrite eruptions and collateral subsidence in the Taupo Volcanic Zone, New Zealand. *Geol. Soc. Am. Bull.* **119**, 18–30 (2007).
33. D. A. Wark, E. B. Watson, TitaniQ: A titanium-in-quartz geothermometer. *Contrib. Mineral. Petrol.* **152**, 743–754 (2006).
34. D. A. Wark, W. Hildreth, F. S. Spear, D. J. Cherniak, E. B. Watson, Pre-eruption recharge of the Bishop magma system. *Geology* **35**, 235–238 (2007).
35. J. B. Thomas, E. Bruce Watson, F. S. Spear, P. T. Shemella, S. K. Nayak, A. Lanzirotti, TitaniQ under pressure: The effect of pressure and temperature on the solubility of Ti in quartz. *Contrib. Mineral. Petrol.* **160**, 743–759 (2010).
36. J. B. Thomas, E. B. Watson, F. S. Spear, D. A. Wark, TitaniQ recrystallized: Experimental confirmation of the original Ti-in-quartz calibrations. *Contrib. Mineral. Petrol.* **169**, 27 (2015).
37. R. Huang, A. Audétat, The titanium-in-quartz (TitaniQ) thermobarometer: A critical examination and re-calibration. *Geochim. Cosmochim. Acta* **84**, 75–89 (2012).
38. A. S. Pamukcu, M. S. Ghiorso, G. A. R. Gualda, The effect of growth rate on the production of Ti-enriched rims of quartz phenocrysts in the Bishop magma bodies. *2015 AGU Fall Meeting* (2015).
39. G. A. R. Gualda, M. S. Ghiorso, Low-pressure origin of high-silica rhyolites and granites. *J. Geol.* **121**, 537–545 (2013).
40. K. M. Cooper, A. J. R. Kent, Rapid remobilization of magmatic crystals kept in cold storage. *Nature* **506**, 480–483 (2014).
41. B. L. A. Charlier, C. J. N. Wilson, J. P. Davidson, Rapid open-system assembly of a large silicic magma body: Time-resolved evidence from cored plagioclase crystals in the Oruanui eruption deposits, New Zealand. *Contrib. Mineral. Petrol.* **156**, 799–813 (2008).
42. I. N. Bindeman, B. Fu, N. T. Kita, J. W. Valley, Origin and evolution of silicic magmatism at Yellowstone based on ion microprobe analysis of isotopically zoned zircons. *J. Petrol.* **49**, 163–193 (2008).
43. K. E. Saunders, D. J. Morgan, J. A. Baker, R. J. Wycoszanski, The magmatic evolution of the Whakamaru supereruption, New Zealand, constrained by a microanalytical study of plagioclase and quartz. *J. Petrol.* **51**, 2465–2488 (2010).
44. C. D. Deering, O. Bachmann, J. Dufek, D. M. Gravelly, Rift-related transition from andesite to rhyolite volcanism in the Taupo Volcanic Zone (New Zealand) controlled by crystal-melt dynamics in mush zones with variable mineral assemblages. *J. Petrol.* **52**, 2243–2263 (2011).
45. J. V. Rowland, C. J. N. Wilson, D. M. Gravelly, Spatial and temporal variations in magma-assisted rifting, Taupo Volcanic Zone, New Zealand. *J. Volcanol. Geotherm. Res.* **190**, 89–108 (2010).
46. C. J. N. Wilson, A. M. Rogan, I. E. M. Smith, D. J. Northey, I. A. Nairn, B. F. Houghton, Caldera volcanos of the Taupo Volcanic Zone, New Zealand. *J. Geophys. Res.* **89**, 8463–8484 (1984).
47. J. W. Cole, D. M. Milner, K. D. Spinks, Calderas and caldera structures: A review. *Earth Sci. Rev.* **69**, 1–26 (2005).
48. S. Tramontano, G. A. R. Gualda, M. S. Ghiorso, Internal triggering of volcanic eruptions: Tracking overpressure regimes for giant magma bodies. *Earth Planet. Sci. Lett.* **472**, 142–151 (2017).
49. P. M. Gregg, S. L. de Silva, E. B. Grosfils, J. P. Parmigiani, Catastrophic caldera-forming eruptions: Thermomechanics and implications for eruption triggering and maximum caldera dimensions on Earth. *J. Volcanol. Geotherm. Res.* **241–242**, 1–12 (2012).
50. P. M. Gregg, E. B. Grosfils, S. L. de Silva, Catastrophic caldera-forming eruptions II: The subordinate role of magma buoyancy as an eruption trigger. *J. Volcanol. Geotherm. Res.* **305**, 100–113 (2015).
51. S. Seitz, B. Putlitz, L. P. Baumgartner, S. Escrig, A. Meibom, A.-S. Bouvier, Short magmatic residence times of quartz phenocrysts in Patagonian rhyolites associated with Gondwana breakup. *Geology* **44**, 67–70 (2016).
52. T. H. Druitt, F. Costa, E. Delouie, M. Dungan, B. Scaillet, Decadal to monthly timescales of magma transfer and reservoir growth at a caldera volcano. *Nature* **482**, 77–80 (2012).
53. G. A. R. Gualda, D. L. Cook, R. Chopra, L. Qin, A. T. Anderson, M. Rivers, Fragmentation, nucleation and migration of crystals and bubbles in the Bishop Tuff rhyolitic magma. *Trans. R. Soc. Edinb. Earth. Sci.* **95**, 375–390 (2004).
54. E. S. Gladney, I. Roelandts, 1987 compilation of elemental concentration data for USGS BHVO-1, MAG-1, QLO-1, RGM-1, SCo-1, SDC-1, SGR-1, and STM-1. *Geostand. Newslett.* **12**, 253–362 (1988).
55. S. R. Sutton, P. M. Bertsch, M. Newville, M. Rivers, A. Lanzirotti, P. Eng, Microfluorescence and microtomography analyses of heterogeneous Earth and environmental materials. *Rev. Mineral. Geochem.* **49**, 429–483 (2002).
56. K. P. Jochum, U. Weis, B. Stoll, D. Kuzmin, Q. Yang, I. Raczek, D. E. Jacob, A. Stracke, K. Birbaum, D. A. Frick, D. Günther, J. Enzweiler, Determination of reference values for NIST SRM 610–617 glasses following ISO guidelines. *Geostand. Geoanal. Res.* **35**, 397–429 (2011).

57. M. Kurosawa, S. E. Jackson, S. Sueno, Trace element analysis of NIST SRM 614 and 616 glass reference materials by laser ablation microprobe-inductively coupled plasma-mass spectrometry. *Geostand. Newslett. J. Geostand. Geoanal.* **26**, 75–84 (2002).
58. W. L. Griffin, W. J. Powell, N. J. Pearson, S. Y. O'Reilly, in *Laser Ablation-ICP-MS in the Earth Sciences* (Mineralogical Association of Canada, 2008), vol. 40, pp. 204–207.
59. A. J. Padilla, G. A. R. Gualda, Crystal-melt elemental partitioning in silicic magmatic systems: An example from the Peach Spring Tuff high-silica rhyolite, Southwest USA. *Chemical Geology* **440**, 326–344 (2016).
60. W. P. Leeman, C. M. MacRae, N. C. Wilson, A. Torpy, C.-T. A. Lee, J. J. Student, J. B. Thomas, E. P. Vicenzi, A study of cathodoluminescence and trace element compositional zoning in natural quartz from volcanic rocks: Mapping titanium content in quartz. *Microsc. Microanal.* **18**, 1322–1341 (2012).
61. D. J. Cherniak, E. B. Watson, D. A. Wark, Ti diffusion in quartz. *Chem. Geol.* **236**, 65–74 (2007).
62. G. A. R. Gualda, M. S. Ghiorso, MELTS_Excel: A Microsoft Excel-based MELTS interface for research and teaching of magma properties and evolution. *Geochem. Geophys. Geosyst.* **16**, 315–324 (2015).
63. M. S. Ghiorso, G. A. R. Gualda, A method for estimating the activity of titania in magmatic liquids from the compositions of coexisting rhombohedral and cubic iron-titanium oxides. *Contrib. Mineral. Petrol.* **165**, 73–81 (2013).

Acknowledgments: We thank members of the MESSY group at Vanderbilt University for suggestions on the manuscript. **Funding:** This work was supported by the NSF (EAR-1151337) and by two Vanderbilt University Discovery Grants. Portions of this work were performed at

GeoSoilEnviroCARS (The University of Chicago, Sector 13), Advanced Photon Source, Argonne National Laboratory. GeoSoilEnviroCARS was supported by the NSF–Earth Sciences (EAR-1128799) and Department of Energy–GeoSciences (DE-FG02-94ER14466). This research used resources of the Advanced Photon Source, a U.S. Department of Energy (DOE) Office of Science User Facility operated for the DOE Office of Science by Argonne National Laboratory under contract no. DE-AC02-06CH11357. **Author contributions:** G.A.R.G. and D.M.G. designed the study. G.A.R.G., D.M.G., M.C., B.H., A.S.P., and F.B. conducted field work and sample collection. A.S.P. and F.B. contributed additional samples. M.C. and B.H. obtained analytical data, with help from and under the supervision of G.A.R.G. M.S.G. performed thermodynamic calculations using rhyolite-MELTS, particularly pressure determinations. C.D.D. contributed knowledge on flare-up volcanism. G.A.R.G. and D.M.G. wrote the paper, and all authors revised it. **Competing interests:** The authors declare that they have no competing interests. **Data and materials availability:** All data needed to evaluate the conclusions in the paper are present in the paper and/or the supplementary materials. Additional data related to this paper may be requested from the authors.

Submitted 23 August 2017

Accepted 31 August 2018

Published 10 October 2018

10.1126/sciadv.aap7567

Citation: G. A. R. Gualda, D. M. Gravley, M. Connor, B. Hollmann, A. S. Pamukcu, F. Bégué, M. S. Ghiorso, C. D. Deering, Climbing the crustal ladder: Magma storage-depth evolution during a volcanic flare-up. *Sci. Adv.* **4**, eaap7567 (2018).